Layered bismuth oxyhalide nanomaterials for highly efficient tumor photodynamic therapy

Yu Xu,†[a] Zhenzhi Shi,†[a,b] Ling'e Zhang,[a] Eric Michael Bratsolias Brown[c] and Aiguo Wu*[a]

Layered bismuth oxyhalide nanomaterials have received much more interest as promising photocatalysts because of their unique layered structures and high photocatalytic performance, which can be used as potential inorganic photosensitizers in tumor photodynamic therapy (PDT). In recent years, photocatalytic materials have been widely used in PDT and photothermal therapy (PTT) as inorganic photosensitizers. This investigation focuses on applying layered bismuth oxyhalide nanomaterials toward cancer PDT, an application that has never been reported so far. The results of our study indicate that the efficiency of UV-triggered PDT was highest when using BiOCl nanoplates followed by BiOCl nanosheets, and then TiO_2. Of particular interest is the fact that layered BiOCl nanomaterials showed excellent PDT effects under low nanomaterial dose (20 μg mL^{-1}) and low UV dose (2.2 mW cm^{-2} for 10 min) conditions, while TiO_2 showed almost no therapeutic effect under the same parameters. BiOCl nanoplates and nanosheets have shown excellent performance and an extensive range of applications in PDT.

1. Introduction

In recent years, layered materials, such as atomically thick graphene, perovskites, layered double hydroxides, have received more and more interest, because they are fundamentally and technologically intriguing for a variety of potential applications in electronics, catalysis, and energy storage.[1–4] Of these layered materials, bismuth oxyhalides BiOX (X═Cl, Br, and I) belong to a new class of promising layered materials for photocatalytic energy conversion and environment remediation because their unique layered-structure mediates fascinating physicochemical properties and a suitable band-structure. As a group of V-VI-VII ternary compound semiconductors, bismuth oxyhalides with a tetragonal matlockite structure crystallize into layered structures consisting of [X–Bi–O–Bi–X] slices stacked together by the nonbonding (van der Waals) interaction through the halogen atoms along the *c*-axis. In each [X–Bi–O–Bi–X] layer, a bismuth center is surrounded by four oxygen and four halogen atoms, which thus generate an asymmetric decahedral geometry.[5] The strong intralayer covalent bonding and the weak interlayer van der Waals interaction give rise to highly anisotropic structural, electrical, optical, and mechanical properties, which endow BiOX with promising potential applications for photocatalytic waste water and indoor-gas purification, water splitting, organic synthesis, and selective oxidation of alcohols.[6–8] With a high photocatalytic performance, the application of bismuth oxyhalides can be extended to a new biomedical application such as tumor photodynamic therapy.

Photodynamic therapy (PDT) is a light triggered method that excites a photosensitizer to generate localized production of singlet oxygen ($^1O_2$), leading to the degradation of nearby unwanted biological agents. Since light irradiation under properly selected parameters does not directly damage neighboring cells or those that have not been exposed to the photosensitizer, PDT can remarkably improve cell selectivity and has fewer side effects compared to conventional chemotherapeutic and radiotherapeutic methods. PDT has been widely studied in recent years to develop new materials, new applications, and new treatment modes for use in cancer therapeutics.[9–12]

As one of the most widely produced and used photocatalytic materials, TiO_2 has been widely researched as a nano-platform for cancer photodynamic therapy. In 2007, Cheon's group reported that they successfully used water-soluble single-crystalline TiO_2 nanoparticles for photocatalytic cancer-cell treatment after the biology of TiO_2-oligonucleotide nanocomposites was reported by Woloschak's group.[13,14] Jiang's group reported that the conjugation of TiO_2 nanoparticles with monoclonal antibodies could increase the photokilling

[a]*Key Laboratory of Magnetic Materials and Devices, & Division of Functional Materials and Nanodevices, Ningbo Institute of Materials Technology and Engineering, Chinese Academy of Sciences, Ningbo, 315201, China. E-mail: aiguo@nimte.ac.cn*
[b]*The Research Institute of Advanced Technologies, Ningbo University, Ningbo 315211, China*
[c]*Department of Biology, North Park University, 3225 W. Foster Ave, Chicago, IL 60625, USA*

selectivity of TiO_2 to cancer cells.[15] Following these early studies, a variety of TiO_2 based nanomaterials were investigated for PDT cancer applications, including TiO_2 sensitized with zinc phthalocyanine (ZnPc), Fe-doped TiO_2 nanocomposites, Fe_3O_4–TiO_2 nanocomposites, TiO_2 PEGDA hybrid hydrogel, mixed phase TiO_2(B)/anatase nanofibers, a combination of gambogic acid with TiO_2 nanofibers, and others.[16–21]

UV triggered photodynamic therapy has a relatively shallow depth of penetration and sufficient levels of ultraviolet light itself may damage normal tissues, which may limit therapeutic applications. But, our research is still meaningful. First, the exploration of new biomaterials with enhanced treatment efficiencies is of obvious importance to both materials science and medicine science, even if UV light ends up being the imperfect irradiation source that is used to excite the nanomaterials. Second, higher treatment efficiencies can decrease the UV power density required so that the side-effects caused by UV light can be reduced. Third, layered bismuth oxyhalide has the potential of also being used in CT imaging.[22] Moreover, our group had reported that the photothermal effect of H-TiO_2 NPs can be attributed to their dramatically enhanced nonradiative recombination.[23] After polyethylene glycol (PEG) coating, H-TiO_2-PEG NPs exhibit a high photothermal conversion efficiency of 40.8%, and stable size distribution in serum solution.[23] These findings demonstrate that infrared-irradiated H-TiO_2-PEG NPs exhibit low toxicity, and high efficiency as potential photothermal agents for cancer therapy.[23] It is likely that this phenomenon can also be applied to our BiOCl nanoplates and nanosheets to further enhance their application in cancer nanotechnology by eliminating the need to use UV light as an excitation source. All these areas deserve additional research and are very relevant for using layered photocatalytic materials for biomedical applications.

Herein, we sought to combine the well-studied advantages of TiO_2 nanomaterials with the recently discovered potential of bismuth oxyhalide nanomaterials to investigate, for the first time, the development of layered bismuth oxyhalide nanomaterials for cancer treatment. We compared the efficiency of photocatalytic degradation of BiOCl nanoplates and nanosheets to TiO_2. Finally, we tested the cellular toxicity of these newly developed nanomaterials and studied the efficacy of their use in the photodynamic therapy of tumor cells (Scheme 1).

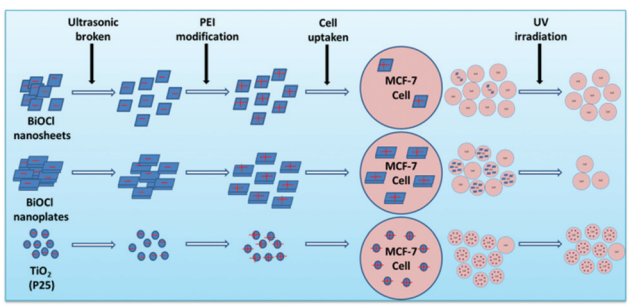

Scheme 1 A scheme of an experimental process in this study.

2. Materials and methods

2.1 Materials

Polyvinylpyrrolidone (PVP) and sodium chloride (NaCl) were purchased from Sinopharm Chemical Reagent Co., Ltd (Beijing, China). Bismuth nitrate pentahydrate ($Bi(NO_3)_3{\cdot}5H_2O$), polyetherimide (PEI) and mannitol were purchased from Aladdin Chemistry Co., Ltd (Shanghai, China). Titanium(IV) oxide (P25) was purchased from ACROS. 3-(4,5-Dimethylthiazol-2-yl)-2,5-diphenyltetrazolium bromide (MTT) and nuclear dyes Hoechst 33258 were obtained from Ningbo Hangjing bio-technology Co., Ltd. (Ningbo, China). Fetal bovine serum (FBS), Dulbecco's modified Eagle's medium (DMEM), penicillin–streptomycin solution, and trypsin-EDTA solution were purchased from Gibco (Grand Island, USA). Milli-Q water (18 MΩ cm) was used for all solution preparations. All chemicals were analytical grades as received.

2.2 Synthesis of BiOCl nanoplates and nanosheets

2.2.1 Synthesis of BiOCl nanoplates. The BiOCl nanoplates (a) were synthesized using a method proposed by Xiong *et al.*[5] According to this protocol, 0.486 g $Bi(NO_3)_3{\cdot}5H_2O$ and 0.455 g mannitol were mixed and dissolved in 25 mL deionized water. After 10 min of stirring and ultrasonic dispersion, 5 mL of saturated NaCl solution was slowly added into the stirring mixture using an injector, and a uniform white suspension was formed. After another 10 min of ultrasonic dispersion, the mixture was transferred into a Teflon-lined stainless steel autoclave of 50 mL capacity, which was heated at 160 °C for 3 h and then cooled down naturally. The resulting product was collected for the following experiment.

2.2.2 Synthesis of BiOCl nanosheets. For the BiOCl nanosheets (b), 0.486 g $Bi(NO_3)_3{\cdot}5H_2O$, 0.400 g PVP, and 0.455 g mannitol were mixed and dissolved in 25 mL deionized water. After 10 min of stirring and ultrasonic dispersion, 5 mL of saturated NaCl solution was slowly added into the stirring mixture using an injector, and a uniform white suspension was formed. After another 10 min of ultrasonic dispersion, the mixture was transferred into a Teflon-lined stainless steel autoclave of 50 mL capacity, which was heated at 160 °C for 3 h and then cooled down naturally. The resulting product was collected for the following experiment.[6]

2.3 Modification of BiOCl nanoplates and nanosheets

The collected products mentioned above (a, b) along with the purchased P25 nanoparticles (c) were separately disposed by ultrasonication for 30 min with the ultrasonic cell disruptor (XC-CD, purchased from Ningbo Yinzhou Forward Electronic Technology Co. Ltd). They were then added into excess amounts of PEI solution. After stirring for 24 h, the solution was washed with deionized water several times to remove the residual PEI molecules; the centrifugal conditions each time were 3000 rpm for 5 min. At the end of this multi-step procedure, modified BiOCl nanoplates (a), BiOCl nanosheets (b) and P25 (c) were obtained.

2.4 Characterization of the prepared nanomaterials

Transmission electron microscopy (TEM) and high-resolution TEM (HRTEM) images were obtained using a JEOL-2100 transmission electron microscope operating at 200 kV. Powder X-ray diffraction (XRD) measurements were performed on a D8 Focus diffractometer (Bruker) with the use of Cu-Kα radiation, operating at 40 kV and 40 mA. Dynamic light scattering (DLS) and zeta-potential experiments were conducted on a Zetasizer Nanoseries (Nano-ZS, Malvern Instruments). Inductively coupled plasma optical emission spectrometry (ICP-OES) was performed with an Optima 2100 instrument from Perkin Elmer. UV-vis absorption spectra were obtained on a PERSEE T100S ultraviolet and visible spectrophotometer.

2.5 Photocatalytic degradation

Photocatalytic activities of the prepared products were evaluated by examining the photodegradation of methyl violet under UV irradiation from a 300 W high-pressure mercury lamp with a 420 nm cutoff filter as the UV source. Typically, 300 μL catalysts (2 μg μL^{-1}) were added into 8 mL of 10^{-5} M methyl violet aqueous solution. Before illumination, the suspension was placed in the dark under constant stirring for 10 min. During the course of this procedure, 1 mL of the suspension was taken out every 5 min under irradiation and centrifuged to remove the photocatalyst for UV–vis absorption spectrum measurements. The concentration of methyl violet was determined by monitoring its characteristic absorption at 583 nm over the indicated time course.

2.6 *In vitro* cytotoxicity of BiOCl nanoplates and nanosheets

The MCF-7 human breast cancer cell line was obtained from Ningbo no. 2 Hospital. The cells were cultured in DMEM supplemented with 10% fetal bovine serum and 1% penicillin–streptomycin in a humidified incubator at 37 °C in air with 5% CO_2. *In vitro* cytotoxicities of BiOCl nanoplates and BiOCl nanosheets were measured through the MTT (3-[4,5-dimethylthiazol-2-yl]-2,5-diphenyl tetrazolium bromide) assay. Typically, 100 μL of MCF-7 cells were seeded in each well of a 96-well plate at a density of 1×10^4 cells per well and incubated for 24 h. Thereafter, the cells were incubated with 100 μL of fresh DMEM with various concentrations of BiOCl nanoplates, BiOCl nanosheets or P25 containing 10% FBS for another 24 h. Subsequently, 10 μL of MTT (5.0 mg mL^{-1} in PBS) was added into each well. After 4 h of incubation, the entire medium with MTT was removed and 100 mL of DMSO was added to each well to dissolve the formed formazan crystals. Finally, the absorbance of each well was measured at 550 nm using a microplate reader (iMark 168-1130, Bio-rad) to calculate the cell viability. For the untreated control group, the same volume of fresh culture medium without nanomaterials was added to the plate. The cell viability of each treatment was compared to the untreated control group and expressed as percentage.

2.7 Cellular uptake using confocal laser scanning microscopy

Before incubation with MCF-7 cells, the nanomaterials were stirred together with an alizarin red solution and washed 3 times with water to enable red fluorescence detection of nanomaterials. MCF-7 cells (1 mL, 1×10^5, determined by a cell counting board) were seeded into 35 mm culture dishes and incubated for 24 h. The growth media were then replaced by fresh DMEM, P25, BiOCl nanoplates, or BiOCl nanosheets. After incubation for 4 h, cells were washed three times with PBS, fixed with 4% formaldehyde for 30 min, washed 3 times with PBS, incubated with 0.2% Triton X-100 for 10 min, and rinsed with PBS again. Next, a 1% BSA solution was added for 25 min to block nonspecific binding sites. The cells were then stained with 200 μL (50 μg mL^{-1}) of FITC-phalloidine for 1 h at 37 °C and washed 3 times with PBS. Finally, the cells were stained with 1 mL of Hoechst 33258 (5 μg mL^{-1}) for 15 min and washed 3 times with PBS. All samples were then imaged with a Leica TCS SP5 confocal microscope (Leica Microsystems, Germany). Excitation and emission wavelengths (nm) used for Hoechst 33258, FITC-phalloidine, and alizarin red were 405 nm/420–480 nm, 488 nm/500–540 nm, and 633 nm/636–721 nm, respectively.

2.8 *In vitro* UV-induced photodynamic therapy

MCF-7 cells were plated in 96-well plates at a density of 1×10^4 cells per well and incubated for 24 h. The existing culture media were then replaced with DMEM containing 10% FBS and either 100 μL of P25, BiOCl nanoplates or BiOCl nanosheets for another 4 h. For the untreated control group, the same volume of fresh culture medium (without a photosensitizer) was added to the plate. After 4 h of incubation, the cells were washed and a fresh cell culture medium was added. The PDT-treated groups were immediately irradiated with a UV-filtered mercury lamp (300 W) at different power densities (full lamp power density, 1/3 lamp power density and 1/10 lamp power density) and irradiation times (5 min, 10 min, 20 min, 30 min). The cells were incubated for another 24 h, and the cell viability was measured using the aforementioned MTT assay. The experimental parameters for the dark controls treated with P25, BiOCl nanoplates, or BiOCl nanosheets were kept identical to the experimental group except for an absence of irradiation. The power densities (mW cm^{-2}) used in the photodynamic therapy experiments were measured with a UV light meter.

3. Results and discussion

3.1 Preparation and characterization of BiOCl nanoplates and nanosheets

We prepared BiOCl nanoplates and BiOCl nanosheets according to the synthesis method proposed by Guan *et al.*[6] but the materials we obtained often precipitated out of solution as shown in Fig. 1. Therefore, we further processed the samples to increase solubility and prevent precipitation. All of these nanomaterials were ultrasonically broken and modified with

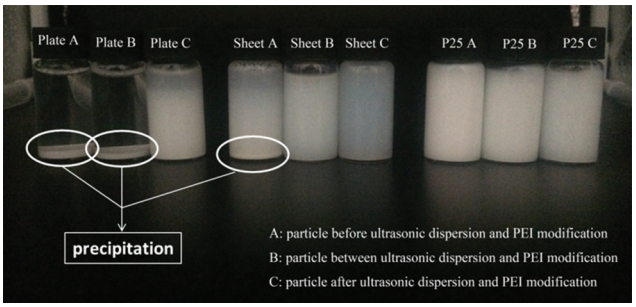

Fig. 1 A schematic representation for the dispersion stability of BiOCl nanoplates, BiOCl nanosheets and P25 is depicted. (A) Nanoparticles before ultrasonic dispersion and PEI modification. (B) Nanoparticles between ultrasonic dispersion and PEI modification. (C) Nanoparticles after ultrasonic dispersion and PEI modification.

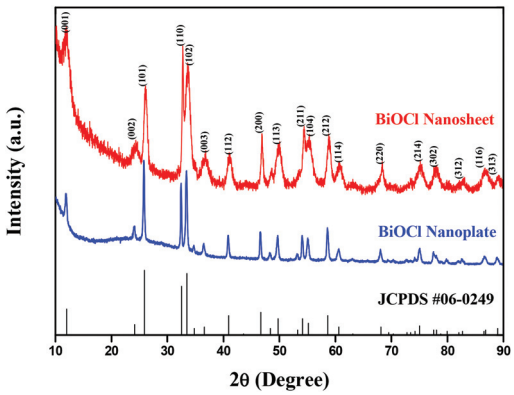

Fig. 3 XRD pattern of BiOCl nanoplates and BiOCl nanosheets; the black lines give the corresponding standard pattern of JCPDS card no.06–0249.

PEI. The results showed that BiOCl nanoplates and BiOCl nanosheets have ideal dispersion stabilities after ultrasonic dispersion and PEI modification, so they may be used for biological applications. The size distribution of BiOCl nanoplates, BiOCl nanosheets and P25 were characterized by Dynamic Light Scattering (DLS) (Nano ZS, Malvern). The results (Fig. 2) showed that they had no substantial difference in size and all of them were nano-sized (180–220 nm).

The XRD pattern (Fig. 3) showed that the samples we prepared were exactly BiOCl. We can also see that the BiOCl nanoplates and the BiOCl nanosheets have different dominant crystal faces ((110) and (001) respectively), which leads to some differences in their photocatalytic properties.[6] The morphology of BiOCl nanoplates, BiOCl nanosheets and P25 was characterized by Transmission Electron Microscopy (TEM) (JEOL2100 HR, JEOL). The TEM images (Fig. 4) showed that both of BiOCl nanoplates and BiOCl nanosheets have square shapes.

We measured the zeta-potential of our nanomaterials in Fig. 5. The results showed that they were negatively charged before PEI modification. Our PEI modification changed BiOCl nanoplates, BiOCl nanosheets and P25 to positively charge

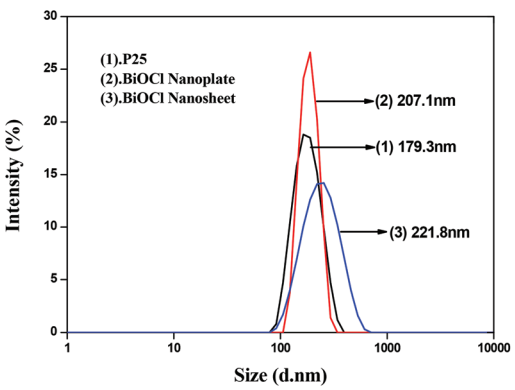

Fig. 2 The dynamic light scattering (DLS) results of P25, BiOCl nanoplates and BiOCl nanosheets.

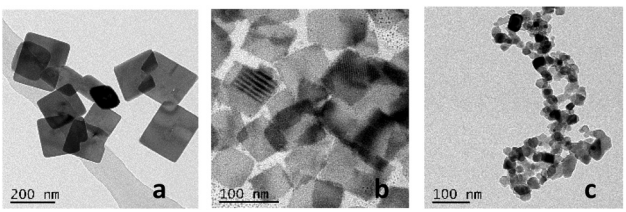

Fig. 4 Characterization of BiOCl nanoplates, BiOCl nanosheets and P25. (a) TEM image of BiOCl nanoplates. (b) TEM image of BiOCl nanosheets. (c) TEM image of P25.

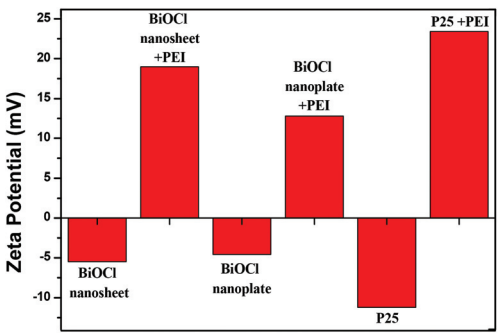

Fig. 5 The zeta potential results of BiOCl nanosheets, BiOCl nanoplates and P25 before and after PEI modification, respectively.

nanomaterials. The UV-Vis-NIR absorption spectra (Fig. 6) showed that both BiOCl nanoplates and BiOCl nanosheets exhibit absorption peaks in the ultraviolet region.

3.2 Photocatalytic degradation of BiOCl nanoplates and nanosheets

In order to further confirm that the nanomaterials we prepared had the potential of a phototherapeutic response in tumor cells, we executed the photocatalytic degradation experiment

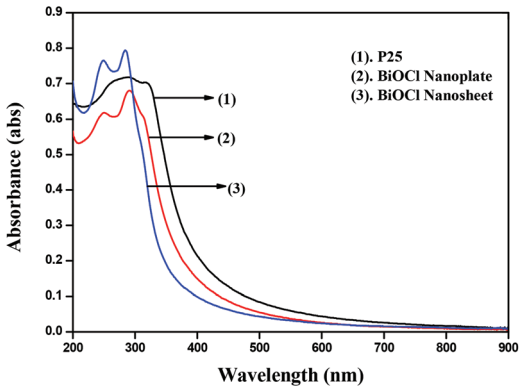

Fig. 6 UV-Vis-NIR absorption spectra of P25, BiOCl nanoplates and BiOCl nanosheets (20 μg mL^{-1}).

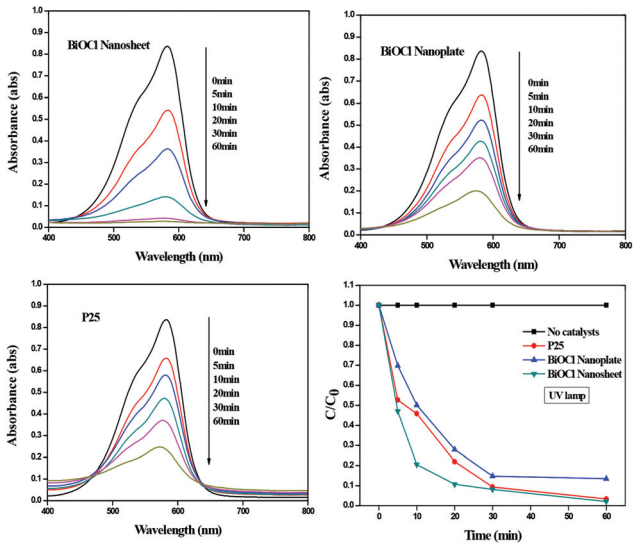

Fig. 7 Photocatalytic activity of BiOCl nanosheets, BiOCl nanoplates and P25. Comparison of photodecomposition of methyl violet with BiOCl nanosheets, BiOCl nanoplates and P25 under UV irradiation.

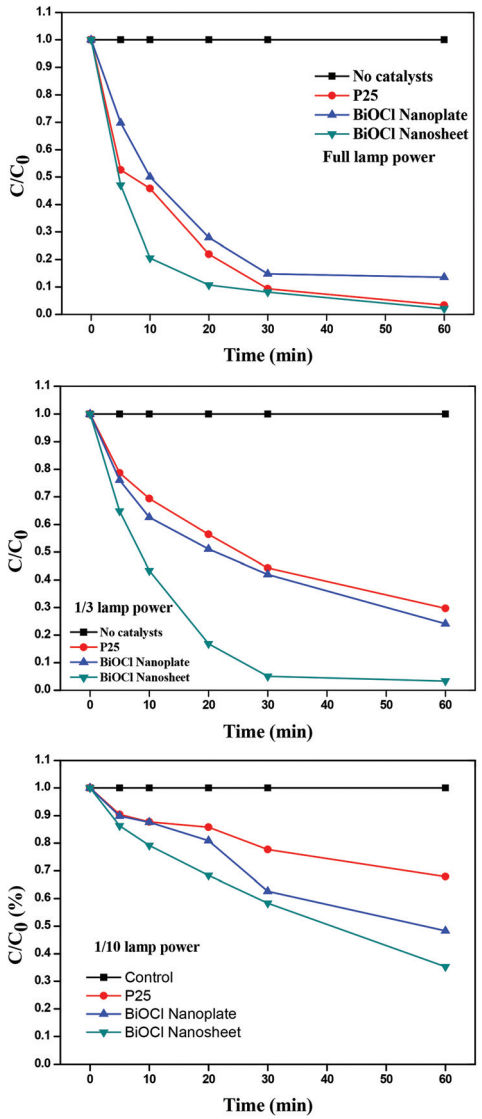

Fig. 8 Comparison of photodecomposition of methyl violet with BiOCl nanosheets, BiOCl nanoplates and P25 under the UV irradiation of three different power densities.

with methyl violet. It is noteworthy that methyl violet is a kind of cationic dye and our BiOCl nanomaterials were positively charged so that we could rule out the influence of dye sensitization catalysis.[6] In other words, here we only focused on the direct catalytic performance of these three nanomaterials. We determined the photocatalytic degradation effect of nanoparticles by observing the change in the characteristic absorption peak intensity of methyl violet. As the results (Fig. 7) showed, both BiOCl nanoplates and BiOCl nanosheets had obvious ultraviolet catalytic degradation abilities. BiOCl nanoplates demonstrated similar degradation performance to P25, while BiOCl nanosheets were superior to both of the aforementioned nanomaterials. Furthermore, it was experimentally ascertained that under short irradiation times, such as 5 min, both BiOCl nanoplates and BiOCl nanosheets were superior to P25. Therefore, we can conclude that layered BiOCl nanomaterials are more sensitive to UV light than P25. In order to verify this conclusion, we used a series of different intensity UV light sources to conduct additional experiments and obtain the results shown in Fig. 8. According to these results, we found in all cases that decreases in UV intensity led to decreases in photocatalytic effects. This phenomenon was more pronounced in P25 than in BiOCl nanomaterials. UV-triggered photocatalytic performance efficiencies were observed in the following order (from most to least): BiOCl nanosheets > BiOCl nanoplates > TiO_2. In other words, when the UV power density was very low, BiOCl had far superior UV catalytic performance than P25. All the above results support the use of our nanomaterials in UV triggered photodynamic therapy of tumors.

3.3 Cell uptake of BiOCl nanoplates and nanosheets

Because the action radius of cytotoxic singlet oxygen is less than 20 nm, the cellular uptake of photosensitizers is of great significance when using photodynamic therapy in cancer cells.[24–26] This suggests that any photosensitizer accumulating in the extracellular space will not function as an effective PDT, even if they accumulate within tumor tissue. To investigate the behavior of intracellular BiOCl nanoplates, BiOCl nanosheets and P25 further, cellular internalization of the photosensitizer was visualized using both optical microscopy and confocal fluorescence microscopy (Ex = 633, Em = 636–721 nm) to evaluate the degree of photosensitizer uptake into the cancer cells and intracellular localization of BiOCl nanomaterials. It is clear that the red fluorescence intensity inside MCF-7 cells treated with P25 was greater than that inside MCF-7 cells treated with BiOCl nanoplates. Cells treated with BiOCl nanosheets demonstrated the weakest red fluorescence signal. The same results were observed from optical microscopy images (Fig. 9). Although cells internalized TiO_2 nanoparticles well, subsequent photodynamic therapy experiments did not yield extraordinary results. This is mainly dependent upon the properties of the photo-induced free radicals that were produced.

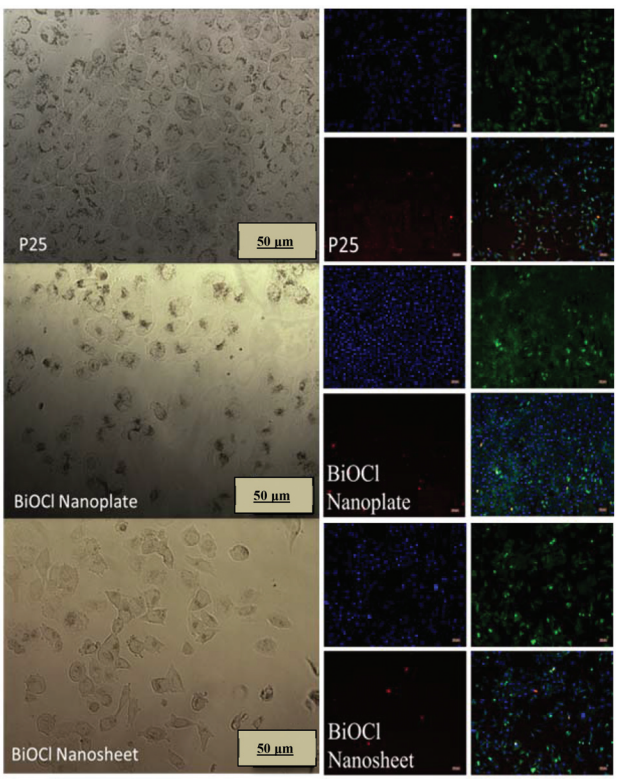

Fig. 9 The optical microscopy images (left) and confocal fluorescence microscopy (right) images of MCF-7 cells incubated with P25, BiOCl nanoplates and BiOCl nanosheets, respectively. Blue fluorescence showed Hoechst 33258 labeled nuclei, green fluorescence indicated FITC–phalloidine stained cell membrane, and red fluorescence was internalization of nanoparticles.

3.4 Cytotoxicity of BiOCl nanoplates and nanosheets in MCF-7 cells

Cell toxicity is another important influencing factor to consider when applying nanomaterials for tumor photodynamic therapy. Thus, *in vitro* cytotoxicity to MCF-7 cells for different concentrations of BiOCl nanoplates, BiOCl nanosheets and P25 was determined through MTT assays. The cytotoxicity to MCF-7 cells increased with increasing concentrations of BiOCl nanoplates, BiOCl nanosheets and P25 (Fig. 10). The cellular viability losses obtained in these studies were not significant (the cell viability was near 90% (100 μg mL^{-1}) and 80% (200 μg mL^{-1})), so these doses of nanoparticles were used in subsequent experiments. UV irradiation toxicity (cell death caused by pure ultraviolet irradiation without the photosensitizer) was also investigated. We performed a series of experiments with varying irradiation intensities and times. We then selected an appropriate irradiation power density (2.2 mW cm^{-2}) and obtained the results shown in Fig. 11. No

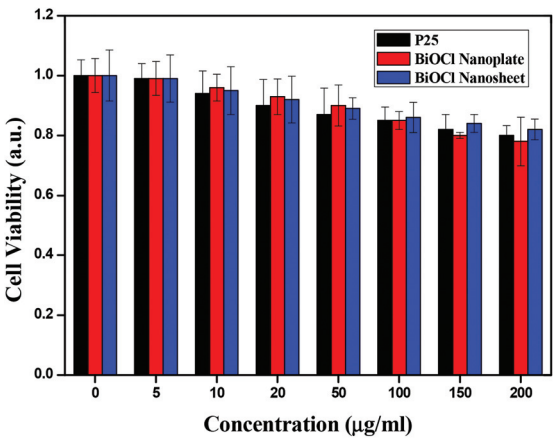

Fig. 10 The cytotoxicity of P25, BiOCl nanoplates and BiOCl nanosheets in MCF-7 cells was measured by an MTT assay (incubation time = 24 h). Data were expressed as the mean ± standard (n = 4).

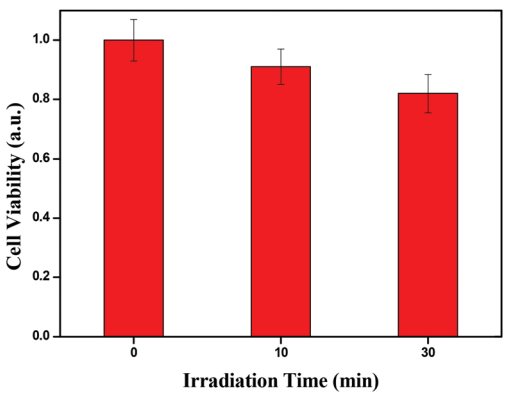

Fig. 11 The viability of MCF-7 human breast cancer cells without incubation with any nanoparticles under the UV irradiation (2.2 mw cm^{-2}) for 0 min, 10 min, 30 min, respectively.

significant viability losses (the cell viability was near 80%) were observed at the irradiation time of 30 min, so this duration of UV irradiation was the maximum used in subsequent experiments.

3.5 BiOCl nanoplates and nanosheets for highly efficient PDT (compared to TiO_2)

On the basis of the aforementioned preliminary experiments, we studied the effect of photodynamic therapy, using BiOCl nanoplates and BiOCl nanosheets, on cancer cells. At the same time, P25 was also investigated as a reference standard, which had been reported in the literature to be effective in producing a photodynamic therapy effect. Under UV light irradiation (2.2 mW cm^{-2}) for different amounts of time (0 min, 10 min, 30 min), the viabilities of MCF-7 cells incubated with different concentrations of BiOCl nanoplates, BiOCl nanosheets or P25 (0, 5, 10, 20, 50, 100, 150, 200 μg mL^{-1}) were investigated using the MTT assay. As shown in Fig. 12, the results showed that BiOCl nanoplates and BiOCl nanosheets had low cytotoxicity when the incubation time was 24 h, which is consistent with the cytotoxicity experimental results mentioned above. However, when they were irradiated under UV light for 10 min, and 30 min, it was observed that the cell viability decreased with increased irradiation time. The concentration of BiOCl nanoplates and BiOCl nanosheets also had an important influence on the cell viability of MCF-7 cells. With an increase in the concentration of BiOCl nanoplates and BiOCl nanosheets, cell viability decreased, and this could be observed clearly even at very low concentrations such as 5, 10, 20, and 50 μg mL^{-1}. When the concentration of BiOCl nanoplates and BiOCl nanosheets was 200 μg mL^{-1}, it was observed that the pre-irradiation cell viability was about 80%, but cell viability was only about 10% and 5% under irradiation times of 10 min and 30 min, respectively. However, under the same conditions, the cell viability of cells that were incubated with P25 was still 80% after UV irradiation for 30 min. At a low concentration of nanoparticles (20 μg mL^{-1}) and short time of UV irradiation (10 min), the cell viability of MCF-7 incubated with BiOCl nanoplates, BiOCl nanosheets and P25 were 35%, 70% and 85% respectively.

The efficiency of the UV triggered photodynamic therapy treatment effect is as follows (from highest to lowest): BiOCl nanoplates > BiOCl nanosheets > TiO_2. According to section 3.3, TiO_2 could be taken up the most by MCF-7 cells, however, TiO_2 showed very low PDT efficiency because of its low UV photocatalytic efficiency as shown in Fig. 8. On the other hand, although BiOCl nanosheets had excellent photocatalytic performance, they were not easily taken up by MCF-7 cells. It is notable that BiOCl nanoplates had the best overall PDT performance because they not only exhibited superior photocatalytic degradation, but also were sufficiently taken up by MCF-7 cells. What demands special attention is the fact that layered BiOCl nanomaterials showed an excellent PDT effect under low nanomaterial dose and low UV dose conditions. In contrast, TiO_2 showed almost no therapeutic effect. Overall, these results indicate that layered bismuth oxyhalide nanomaterials demonstrate significantly better PDT capabilities than TiO_2. Furthermore, among layered bismuth oxyhalide nanomaterials, BiOCl nanoplates exhibit slightly higher PDT capabilities than BiOCl nanosheets.

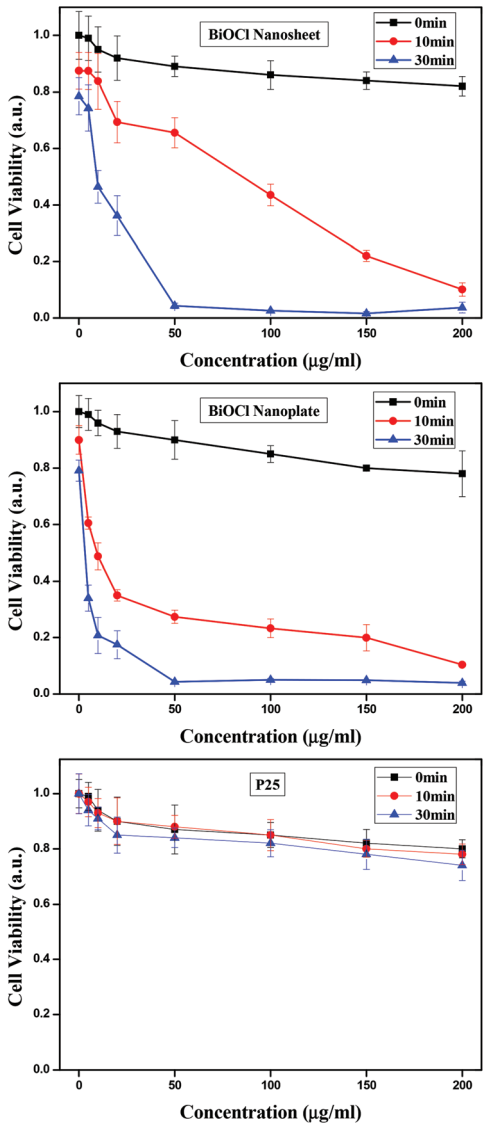

Fig. 12 The UV triggered photodynamic therapy results of BiOCl nanosheets, BiOCl nanoplates and P25.

4. Conclusions

In summary, we successfully prepared two kinds of layered bismuth oxyhalide nanomaterials (BiOCl nanoplates and BiOCl nanosheets) with a simple improved hydrothermal synthesis method. After simple ultrasonic dispersion and PEI modification, we successfully applied them to photodynamic therapy of cancer. The BiOCl nanoplates and BiOCl

nanosheets (200 μg mL^{-1}) achieved high PDT efficacies (about 90% tumor cell killing) under UV irradiation (2.2 mW cm^{-2}, 30 min), while no significant viability loss was induced by TiO_2 under the same irradiation conditions. Additionally, while ensuring the therapeutic effect, a low UV power density (2.2 mW cm^{-2}) reduces the treatment risk. Under a low concentration (20 μg mL^{-1}) and short UV irradiation time (10 min), BiOCl nanoplates and BiOCl nanosheets kill cancer cells with remarkable efficacy (65% and 30% respectively). Our research results showed that the efficiency of UV triggered tumor photodynamic therapy was as follows (highest to lowest): BiOCl nanoplates > BiOCl nanosheets > TiO_2. We speculate that the varying efficiencies of these three nanomaterials are determined by multiple factors. First, they have different electronic band structures, which results in different responses to UV irradiation of varying power densities. Second, they have different crystal morphologies including sphere, plate and sheet, which is an important factor influencing their uptake efficacy by cells. Moreover, there's another significant difference between BiOCl nanoplates and BiOCl nanosheets; they have different dominating crystal faces ((110) and (001)), respectively, which has a strong impact on their PDT efficacies.

Acknowledgements

This work was supported by the National Natural Science Foundation of China (Grant No. U1432114 and 81401452), by Key Breakthrough Program of Chinese Academy of Sciences (KGZD-EW-T06), and by the Hundred Talents Program of Chinese Academy of Sciences (2010-735), Science & Technology Bureau of Ningbo City (2014A610158, 2015C50004 and 2015B11002).

References

1 D. Golberg, Y. Bando, Y. Huang, T. Terao, M. Mitome, C. Tang and C. Zhi, *ACS Nano*, 2010, **4**, 2979–2993.
2 V. Nicolosi, M. Chhowalla, M. G. Kanatzidis, M. S. Strano and J. N. Coleman, *Science*, 2013, **340**(6139), 1226419.
3 M. Chhowalla, H. S. Shin, G. Eda, L.-J. Li, K. P. Loh and H. Zhang, *Nat. Chem.*, 2013, **5**, 263–275.
4 A. K. Geim and I. V. Grigorieva, *Nature*, 2013, **499**, 419–425.
5 J. Xiong, G. Cheng, G. Li, F. Qin and R. Chen, *RSC Adv.*, 2011, **1**, 1542–1553.
6 M. L. Guan, C. Xiao, J. Zhang, S. J. Fan, R. An, Q. M. Cheng, J. F. Xie, M. Zhou, B. J. Ye and Y. Xie, *J. Am. Chem. Soc.*, 2013, **135**, 10411–10417.
7 W. J. Kim, D. Pradhan, B.-K. Min and Y. Sohn, *Appl. Catal., B*, 2014, **147**, 711–725.
8 K. Zhao, L. Zhang, J. Wang, Q. Li, W. He and J. J. Yin, *J. Am. Chem. Soc.*, 2013, **135**, 15750–15753.
9 Z. Shi, W. Ren, A. Gong, X. Zhao, Y. Zou, E. M. B. Brown, X. Chen and A. Wu, *Biomaterials*, 2014, **35**, 7058–7067.
10 A. Yuan, X. L. Tang, X. F. Qiu, K. Jiang, J. H. Wu and Y. Q. Hu, *Chem. Commun.*, 2015, **51**, 3340–3342.
11 A. Kamkaew, S. H. Lim, H. B. Lee, L. V. Kiew, L. Y. Chung and K. Burgess, *Chem. Soc. Rev.*, 2013, **42**, 77–88.
12 A. Master, M. Livingston and A. Sen Gupta, *J. Controlled Release*, 2013, **168**, 88–102.
13 T. Paunesku, T. Rajh, G. Wiederrecht, J. Maser, S. Vogt, N. Stojicevic, M. Protic, B. Lai, J. Oryhon, M. Thurnauer and G. Woloschak, *Nat. Mater.*, 2003, **2**, 343–346.
14 J.-W. Seo, H. Chung, M.-Y. Kim, J. Lee, I.-H. Choi and J. Cheon, *Small*, 2007, **3**, 850–853.
15 J. Xu, Y. Sun, J. J. Huang, C. M. Chen, G. Y. Liu, Y. Jiang, Y. M. Zhao and Z. Y. Jiang, *Bioelectrochemistry*, 2007, **71**, 217–222.
16 T. Lopez, E. Ortiz, M. Alvarez, J. Navarrete, J. A. Odriozola, F. Martinez-Ortega, E. A. Paez-Mozo, P. Escobar, K. A. Espinoza and I. A. Rivero, *Nanomedicine*, 2010, **6**, 777–785.
17 L. Y. Zeng, W. Z. Ren, L. C. Xiang, J. J. Zheng, B. Chen and A. G. Wu, *Nanoscale*, 2013, **5**, 2107–2113.
18 H. Zhang, R. H. Shi, A. J. Xie, J. C. Li, L. Chen, P. Chen, S. K. Li, F. Z. Huang and Y. H. Shen, *ACS Appl. Mater. Interfaces*, 2013, **5**, 12317–12322.
19 S. C. Zhang, D. J. Yang, D. W. Jing, H. W. Liu, L. Liu, Y. Jia, M. H. Gao, L. J. Guo and Z. Y. Huo, *Nano Res.*, 2014, **7**, 1659–1669.
20 S. S. Lucky, N. M. Idris, Z. Li, K. Huang, K. C. Soo and Y. Zhang, *ACS Nano*, 2015, **9**, 191–205.
21 Z. Hou, Y. Zhang, K. Deng, Y. Chen, X. Li, X. Deng, Z. Cheng, H. Lian, C. Li and J. Lin, *ACS Nano*, 2015, **9**, 2584–2599.
22 O. Rabin, J. M. Perez, J. Grimm, G. Wojtkiewicz and R. Weissleder, *Nat. Mater.*, 2006, **5**, 118–122.
23 W. Ren, Y. Yan, L. Zeng, Z. Shi, A. Gong, P. Schaaf, D. Wang, J. Zhao, B. Zou, H. Yu, G. Chen, E. M. B. Brown and A. Wu, *Adv. Healthcare Mater.*, 2015, **4**, 1526–1536.
24 B. Jang, J.-Y. Park, C.-H. Tung, I.-H. Kim and Y. Choi, *ACS Nano*, 2011, **5**, 1086–1094.
25 W. M. Sharman, J. E. van Lier and C. M. Allen, *Adv. Drug Delivery Rev.*, 2004, **56**, 53–76.
26 J. Moan and K. Berg, *Photochem. Photobiol.*, 1991, **53**, 549–553.